PNAS RESEARCH ARTICLE | NEUROSCIENCE

Altered integration of excitatory inputs onto the basal dendrites of layer 5 pyramidal neurons in a mouse model of Fragile X syndrome

Diana E. Mitchell[a,b,1], Soledad Miranda-Rottmann[a,b,1], Maxime Blanchard[a], and Roberto Araya[a,b,2]

Edited by Mark Nelson, University of Vermont, Burlington, VT; received May 25, 2022; accepted November 11, 2022

Layer 5 (L5) pyramidal neurons receive predictive and sensory inputs in a compartmentalized manner at their apical and basal dendrites, respectively. To uncover how integration of sensory inputs is affected in autism spectrum disorders (ASD), we used two-photon glutamate uncaging to activate spines in the basal dendrites of L5 pyramidal neurons from a mouse model of Fragile X syndrome (FXS), the most common genetic cause of ASD. While subthreshold excitatory inputs integrate linearly in wild-type animals, surprisingly those with FXS summate sublinearly, contradicting what would be expected of sensory hypersensitivity classically associated with ASD. We next investigated the mechanism underlying this sublinearity by performing knockdown of the regulatory β4 subunit of BK channels, which rescued the synaptic integration, a result that was corroborated with numerical simulations. Taken together, these findings suggest that there is a differential impairment in the integration of feedforward sensory and feedback predictive inputs in L5 pyramidal neurons in FXS and potentially other forms of ASD, as a result of specifically localized subcellular channelopathies. These results challenge the traditional view that FXS and other ASD are characterized by sensory hypersensitivity, proposing instead a hyposensitivity of sensory inputs and hypersensitivity of predictive inputs onto cortical neurons.

layer 5 pyramidal neurons | synaptic integration | autism spectrum disorders | BK channels | dendritic spines

Significance

Fragile X syndrome (FXS) is the most commonly known cause of autism spectrum disorders (ASD). We found that while control animals integrate subthreshold feedforward excitatory inputs linearly, this integration is sublinear in FXS mice, a defect that was reversed by genetic manipulation of BK channel activity. The sublinear integration contradicts what would be expected of sensory hypersensitivity classically associated with ASD. These findings instead support a model of FXS encompassing sensory hyposensitivity and predictive hypersensitivity at the level of cortical neurons. Moreover, these results highlight the need to study, in FXS and other forms of ASD, channelopathies in cortical feedforward and feedback pathways independently, their associations, and how cortical pyramidal neurons output is affected, which ultimately shapes behavior.

Fragile-X syndrome (FXS) is the most frequent form of inherited intellectual disability and the commonest known cause of autism (1, 2). FXS and other neurodevelopmental disorders associated with autism spectrum disorders (ASD) have a negative impact in most, if not all, everyday life activities, with a global prevalence that has been growing steeply since the 1990s (3). FXS occurs because of the inactivation of the Fragile X Mental Retardation 1 (FMR1) gene, which encodes the FXS Protein (FMRP), a polyribosome-associated RNA-binding protein that inhibits the translation of bound messenger (m)RNAs, especially at synapses (4, 5). At the cellular level, it has been shown that spines [tiny protrusions covering the dendrites of cortical pyramidal and spiny stellate neurons that constitute the postsynaptic element of ~95% of all the excitatory synapses (6–8)] are abnormally long and dense in mice models of FXS (*Fmr1*-knockout (KO) mice) (9, 10). These synaptic alterations suggest the presence of defects in the transmission, plasticity, and integration of excitatory inputs in FXS (11, 12). At the circuit level, the neocortex of *Fmr1*-KO mice has been found to be hyperexcitable (13–17) with pyramidal neurons exhibiting abnormally high and synchronous firing, leading to recurrent bursting (18)—something long assumed to cause sensory hypersensitivity (reviewed in ref. 19).

A key function of the neocortex is to associate external sensory information with an internal representation of the world to make predictions about the future (20–22). Specifically, layer 5 (L5) pyramidal neurons integrate sensory inputs (feedforward) in their basal dendrites with information from other cortical areas (feedback) at the apical dendrites in layer 1 (20). Feedback information provides contextual or internal invariant predictive representation of the world built from previous experiences, while feedforward inputs provide external sensory information. Thus, to make predictions about the world (cognition and conscious perception) the brain has to combine aspects of perceived experience (sensory feedforward information) with an internal representation of the world (predictive feedback information) (23–26). L5 pyramidal neurons, vertically spanning all cortical layers, are the main candidates believed to perform this task (20, 27). Hence, defects in the processing and integration of excitatory inputs at the level of single dendritic spines in the basal and/or distal apical tuft dendrites of L5 pyramidal neurons could contribute to the functional cortical defects associated with neurological disorders such as FXS and ASD. Indeed, previous work has shown during repetitive electrical stimulation of layer 1,

Author contributions: D.E.M., S.M.-R., and R.A. designed research; D.E.M., S.M.-R., and M.B. performed research; D.E.M., S.M.-R., M.B., and R.A. analyzed data; and D.E.M., S.M.-R., and R.A. wrote the paper.

The authors declare no competing interest.

This article is a PNAS Direct Submission.

[1]D.E.M. and S.M.-R. contributed equally to this work.

[2]To whom correspondence may be addressed. Email: roberto.araya@umontreal.ca.

This article contains supporting information online at https://www.pnas.org/lookup/suppl/doi:10.1073/pnas.2208963120/-/DCSupplemental.

Published January 3, 2023.

an enhanced temporal summation of excitatory inputs in the apical dendrites of *Fmr1*-KO L5 pyramidal neurons (13). In addition, this work also found an increase in the number of action potentials, evoked during tactile stimulation, in *Fmr1*-KO L5 pyramidal neurons compared with those in wild-type (WT) neurons (13). It remains unknown, however, how sensory inputs are processed at the level of individual synapses in the basal dendrites of *Fmr1*-KO L5 pyramidal neurons, and whether the synaptic integration impairments are equally or differentially affected within feedforward and feedback pathways in L5 pyramidal neurons in FXS.

Here, we aim to uncover if the integration of feedforward sensory inputs at the level of single synapses in the basal dendrites of L5 pyramidal neurons is altered in *Fmr1*-KO mice and, if so, explore the underlying mechanisms responsible for any observed differences. To do so, we first determined how near-simultaneous inputs onto neighboring spines are integrated in L5 pyramidal neuron dendrites from *Fmr1*-KO versus WT mice. As previously demonstrated (28), we found that the basal dendrites of WT L5 pyramidal neurons integrate inputs linearly before the generation of a dendritic spike, whereas, surprisingly, synaptic inputs in L5 pyramidal neuron basal dendrites summate sublinearly in *Fmr1*-KO mice. To try to understand the underlying mechanism, we focused on spine channelopathies that have been associated with FXS (29), in particular defects in large-conductance voltage- and calcium-activated potassium (BK) channels that have been described in the apical dendrites of *Fmr1*-KO L5 pyramidal neurons (13). Previous work has further revealed that FMRP interacts with the β4 regulatory subunit of BK channels (30), which are localized to dendritic spines where they play a role contributing to synaptic efficacy in L5 pyramidal neurons (31). Thus, in WT mice, FMRP can sequester the β4 subunit, as has been shown in the hippocampal pyramidal neurons (30), and prevent it from interacting with BK channels, whereas in *Fmr1*-KO animals, an increased binding of BK channels and its β4 subunit would occur. The β4 subunit decreases the probability of BK channels opening at low calcium concentrations and increases it at high calcium concentrations while also slowing down activation and deactivation kinetics (32, 33), which would ultimately affect L5 pyramidal neuron integrative properties. Hence, we predicted that the sublinear integration in the basal dendrites of *Fmr1*-KO L5 pyramidal neurons was due to altered BK channel activity via its interaction with the β4 subunit in the absence of FMRP and subsequent increased dendritic repolarization when two spines are activated, compared with WT neurons. Here, we found that knockdown of the β4 subunit of BK channels, using short hairpin RNA (shRNA), rescues the linear integration of subthreshold inputs in the basal dendrites of *Fmr1*-KO L5 pyramidal neurons while injection of a scrambled version has no effect. Numerical simulations corroborate these experimental results, showing that synaptic integration occurs linearly only when the kinetics of the α-subunit of spine BK channels are modeled, while the β4 subunit boosted the number of open BK channels per spine, leading to a greater repolarization and sublinear integration of subthreshold excitatory inputs in the basal dendrites of *Fmr1*-KO L5 pyramidal neurons. Taken together, our findings support a model of FXS that is more intricate than one simply characterized by a global cortical hypersensitivity, and help to uncover the role of ion channels in excitatory input integration to identify localized dendritic targets for the design of specific treatment options to alleviate symptoms associated with FXS.

Results

Sublinear Integration of Synaptic Inputs in the Basal Dendrites of L5 Pyramidal Neurons in *Fmr1*-KO Mice. To study synaptic integration in the basal dendrites of L5 pyramidal neurons in acute brain slices of the mouse visual cortex from WT and *Fmr1*-KO mice, we applied two-photon (2P) uncaging of caged glutamate (4-methoxy-7-nitroindolinyl glutamate (MNI)-glutamate, 2.5 mM; see *Methods*) at two individual spines separately and then together near-simultaneously (Fig. 1*A*). Whole-cell patch clamp recordings in current-clamp were performed to measure the uncaging (u)-evoked excitatory postsynaptic potentials (uEPSP) at the soma. This technique allows for the precise activation of individual dendritic spines with responses that are similar to those from physiological activation of single synapses (28, 31, 34–41). As shown previously (28), subthreshold synaptic inputs onto spines in the basal dendrites of WT L5 pyramidal neurons integrate linearly (Fig. 1*A*). Specifically, we found that activating individual spines triggered uEPSPs (black traces in *Upper* panel of Fig. 1*A*), which added linearly to accurately predict the response when two spines were activated near-simultaneously (compare black and blue dashed traces in the *Upper Right* panel of Fig. 1*A*). We quantified these results by calculating linearity indices, using either the peak or integral of the uEPSP as well as a gain measure (see *Methods*). Linearity indices were not significantly different from 100% for WT L5 pyramidal neurons when we considered each experiment individually (100.45 ± 1.74%, $P = 0.78$, for peak uEPSP, and 102.82 ± 2.15% $P = 0.20$ for uEPSP integral, Wilcoxon test, n = 40 spine pairs; Fig. 1*B*) or when we averaged each individual experiment per mouse (98.35 ± 2.82%, $P = 0.49$, Wilcoxon test, n = 10 mice for peak uEPSP, and 99.90 ± 3.79% $P = 0.32$, Wilcoxon test, n = 10 mice for uEPSP integral; Fig. 1*C*). We next computed a gain measure, which compares the time-varying uEPSP in response to the activation of two spines to that predicted from the linear summation of individual responses, with a measure of one being a perfect match. We found that the gain measure was not significantly different from the one for WT L5 pyramidal neurons (individual experiments: 1.03 ± 0.02, $P = 0.29$, n = 40 spine pairs; average per mouse: 1.00 ± 0.02, $P = 0.98$, n = 10 mice; Wilcoxon test, Fig. 1 *B* and *C*). Surprisingly, we observed uEPSP responses that were smaller in amplitude and integral than expected based on the sum of individual responses in *Fmr1*-KO mice (compare red and blue dashed traces in the *Lower Right* panel of Fig. 1*A*) with linearity indices significantly lower than 100% (individual experiments: 91.27 ± 1.47%, $P < 0.0001$ for peak uEPSP and 89.58 ± 1.90%, $P < 0.0001$ for uEPSP integral, Wilcoxon test, n = 74 spine pairs; average per mice: 88.56 ± 1.79%, $P < 0.0001$ for peak uEPSP and 88.28 ± 1.89%, $P < 0.0001$ for uEPSP integral, Wilcoxon test, n = 16 mice; Fig. 1 *B* and *C*) and the gain measure significantly lower than one (individual experiments: 0.89 ± 0.02, $P < 0.0001$, n = 74 spine pairs, Wilcoxon test; average per mice: 0.87 ± 0.03, $P < 0.001$, n = 16 mice, Wilcoxon test; Fig. 1 *B* and *C*). These results were surprising, since they contradict what would be expected from a hyperexcitable cortex that has been described in FXS.

We found no difference in the intrinsic cellular properties between *Fmr1*-KO versus WT L5 pyramidal neurons (*SI Appendix*, Fig. S1), except for a significantly longer full width at half maximum (FWHM) of the action potential waveform in *Fmr1*-KO L5 pyramidal neurons compared to WT (*SI Appendix*, Fig. S1*F*). When we activated one (individual) versus two (combined) spines, we found that individual and combined uEPSP responses were smaller in the basal dendrites of *Fmr1*-KO versus WT L5 pyramidal neurons (*SI Appendix*, Fig. S2). This effect was washed out, however, when experiments were pooled per mouse (*SI Appendix*, Fig. S2). Thus, in some animals, there was an overrepresentation of experiments yielding smaller uEPSP sizes. The morphology of activated spines was comparable for *Fmr1*-KO and WT mice

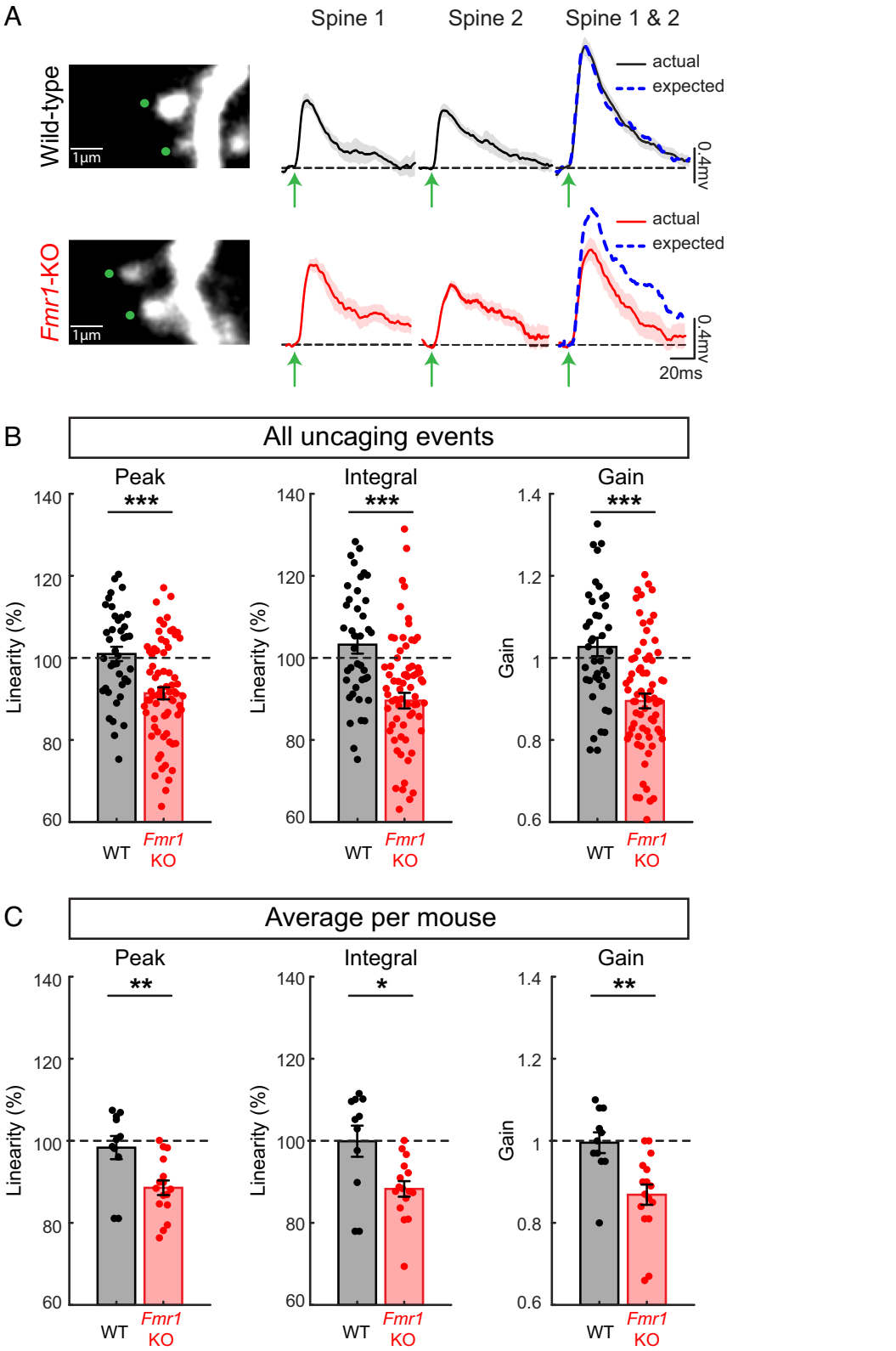

Fig. 1. Sublinear summation of excitatory synaptic inputs in basal dendrites of *Fmr1*-KO L5 pyramidal neurons. (*A*) Representative basal dendrite selected for 2P glutamate uncaging to activate spines from WT (*Top*) and *Fmr1*-KO L5 pyramidal neurons (*Bottom*). Green dots indicate the site for uncaging. Spines were first activated individually (Spine 1 or Spine 2) and then together (Spine 1 & Spine 2). Blue dashed traces correspond to the linear sum of individual events of each spine. (*B*) Observed response has smaller amplitude, integral and gain than expected based on the sum of individual responses in *Fmr1*-KO mice, while in WT mice, the responses summate linearly. (*C*) As in *B*, but values were averaged per mouse.

(*SI Appendix*, Fig. S2) as has been previously reported for this age range (42). Moreover, spine density is also similar in WT and *Fmr1*-KO L5 pyramidal neurons by age P14 (42). Overall, these data indicate that the sublinear integration in *Fmr1*-KO L5 pyramidal neurons cannot be explained by changes in intrinsic cellular properties or spine morphology.

Expression of BK Channel and Its β4-Subunit in the Neocortex of WT Versus *Fmr1*-KO Mice: Neocortical Excitatory Synaptic Enrichment of the β4-Subunit in *Fmr1*-KO Mice. We next sought to identify the mechanism for this sublinear integration of spine activation in the basal dendrites of *Fmr1*-KO L5 pyramidal neurons. Large conductance calcium-activated potassium (BK) channels are homogeneously distributed along the dendritic tree of L5 pyramidal neurons and are believed to play an important role in synaptic transmission and integration (31, 43). BK channels are high-conductance potassium channels formed by a tetramer of α subunits. Membrane depolarization and intracellular calcium activate these channels, and in many tissues auxiliary subunits modulate their kinetics (reviewed in: 44). For example, it has been demonstrated in hippocampal CA3 pyramidal neurons that FMRP modulates BK channel activity by sequestering its regulatory β4 subunit (30). The β4 subunit decreases the probability of BK channel openings at low calcium concentrations but increases the probability of channel openings at high calcium concentrations while also slowing down activation and deactivation kinetics (32, 33). We thus predicted that *Fmr1*-KO L5 pyramidal neurons exhibit altered BK channel activity in the absence of FMRP, compared with WT neurons, which would ultimately affect L5 pyramidal neuron integrative properties. Using Western blot analysis of total protein (TP) and synaptoneurosomes (SN) prepared from the visual cortex, we show that αBK subunits are enriched in synapses, and there is no expression difference between WT and *Fmr1*-KO mice (WT: 1.00 ± 0.13 in SN versus 7.31 ± 0.31 in TP; KO: 1.54 ± 0.09 in SN versus 7.31 ± 0.44 in TP, n = 3, $P < 0.001$, ANOVA) (Fig. 2 *A* and *B*). By contrast, β4 subunits are not enriched in synapses in WT mice but are enriched in those of *Fmr1*-KO mice (WT: 0.90 ± 0.19 in SN versus 0.51 ± 0.09 in TP; *Fmr1*-KO: 1.04 ± 0.36 in SN versus 2.26 ±0.17 in TP, n = 3, $P < 0.05$, $P < 0.0001$, ANOVA) (Fig. 2 *C* and *D*). This increase in β4 immunoreactivity in cortical synapses of *Fmr1*-KO versus WT mice is consistent with FMRP sequestering the β4 regulatory subunit, preventing its interaction with BK channels. To demonstrate that FMRP also interacts with β4 in the visual cortex, we designed an assay of coimmunoprecipitation (co-IP) where FMRP can only be detected if it is pulled down by interaction with β4 (Fig. 2*E*, diagram). The assay demonstrates a specific interaction of FMRP with β4 in the mouse visual cortex (Fig. 2*E*). In addition, immunofluorescence data in transgenic mice expressing green fluorescent protein (GFP) in L5 pyramidal neurons show that αBK (Fig. 2*F*) and β4 (Fig. 2*G*) subunits are present in basal dendrites and spines from WT and *Fmr1*-KO L5 pyramidal neurons, consistent with our previous immunoelectron microscopy findings showing that αBK subunits are localized to dendritic spines in the basal dendrites from L5 pyramidal neurons with nanoscale resolution (31). Interestingly, quantitative image analyses of 3D dendrite reconstructions (Fig. 2*H*) show an increase in the β4 signal intensity in dendritic spines of *Fmr1*-KO compared with WT L5 pyramidal neurons (WT: 3.22 ± 0.29%, n = 143; KO: 6.05 ± 0.68%, n = 206, $P = 0.015$. Mann-Whitney test; Fig. 2*I*) while the total number of spines with detectable levels of β4 immunoreactivity remains unchanged (WT: 47.00 ± 8.44%; KO: 36.00 ± 3.81%, n = 5, $P = 0.31$. Mann–Whitney test). Taken together, these experiments, along with previous findings, provide evidence that BK channel activity and its interaction and regulation by the β4 subunit in cortical spines from *Fmr1*-KO L5 pyramidal neurons might be at the core of the altered integration of synaptic inputs in these neurons.

Knock-Down of BK Channel β4 Subunit in L5 Pyramidal Neurons of *Fmr1*-KO Mice Rescues the Subthreshold Linear Integration of Synaptic Inputs. In order to test the hypothesis that the lack of FMRP in *Fmr1*-KO mice leads to an elevated binding of the β4 subunit to BK channels in spines and dendrites, thus disrupting the linearity of incoming synaptic inputs, we performed a knockdown of the β4 subunit of BK channels, using shRNA in *Fmr1*-KO L5 pyramidal neurons (Fig. 3*A*). Two shRNA sequences recognizing the open reading frame of the mouse kcnmb4 gene encoding the β4 subunit (β4shRNA, see *Methods*) were inserted into a viral vector to produce adeno associated virus (AAV) (Fig. 3*A*). The efficiency of the β4shRNA was first validated in mouse brain by IP-western blot showing a ~50% reduction in β4 protein consistent with sparse neuronal expression observed during imaging (*SI Appendix*, Fig. S3 *A–C*) and in 293T cells analyzed by qRT-PCR showing a significant β4 mRNA expression inhibition (*SI Appendix*, Fig. S3 *D* and *E*, control: 100.67 ± 9.68%, β4shRNA: 43.33 ± 1.45%, $P = 0.0042$, unpaired *t* test) with 31.09 ± 4.29% of β4-expressing cells also expressing β4shRNA, assessed by fluorescent image analysis (*SI Appendix*, Fig. S3 *F–G*).

Mice were injected with β4shRNA-expressing AAVs at postnatal day 18, and 2 wk later we performed 2P uncaging of caged glutamate at two individual spines separately and then together near-simultaneously as described above. Analyzing each experiment individually, we found that expression of β4shRNAs rescued the subthreshold linear integration of synaptic inputs in the basal dendrites of *Fmr1*-KO L5 pyramidal neurons whereas the expression of a nonspecific scrambled version of the shRNA did not (peak linearity: 106.64 ± 2.62 versus 86.61 ± 4.51%, $P = 0.001$; integral linearity: 103.37 ± 2.88 versus 85.93 ± 5.17%, $P = 0.0082$; gain linearity: 1.13 ± 0.06 versus 0.87 ± 0.05, $P = 0.0063$; Mann–Whitney test; Fig. 3 *B–D*). Similar results were found when the average per mouse was instead considered (peak linearity: 105.36 ± 4.47 versus 88.02 ± 4.68%, $P = 0.03$; integral linearity: 106.28 ± 3.66 versus 87.67 ± 4.63%, $P = 0.0017$; gain linearity: 1.20 ± 0.09 versus 0.89 ± 0.06, $P = 0.0017$; Mann-Whitney test; Fig. 3*E*). Moreover, we found no significant difference between linear indices calculated from experiments in L5 pyramidal neurons from *Fmr1*-KO mice expressing β4 subunit shRNA versus those performed on WT L5 pyramidal neurons (individual experiments: peak linearity: $P = 0.18$; integral linearity: $P = 0.99$; gain linearity: $P = 0.12$; Mann-Whitney test; *SI Appendix*, Fig. S4 *E–G*).

Since activity-dependent spine morphological changes [spine head: (45), neck: (36, 38) or both: (46)] have been correlated with synaptic efficacy by altering the biochemical and electrical spine properties (reviewed in: 40), we analyzed spine shape in mice transfected with either the β4 subunit shRNA (β4shRNA) or the scramble shRNA. We found that spine head volume and neck length, as well as spine density remained the same in the basal dendrites of *Fmr1*-KO L5 pyramidal neurons transduced with shRNA against the β4 subunit of BK channels (β4shRNA) versus the scrambled version (spine density: 5.6 ± 1.4, n = 10 images versus 4.1 ± 0.5 spines per 10 μm, n = 12 images; $P = 0.432$; spine head volume: 0.18 ± 0.02, n = 30 spines, versus 0.19 ± 0.03 μm^3, n = 28 spines, $P = 0.932$; neck length: 0.50 ± 0.05, n = 33 spines, versus 0.60 ± 0.05 μm, n = 34 spines, $P = 0.096$, Mann–Whitney test; Fig. 3 *F* and *G*). We also found no difference in the intrinsic cellular properties between *Fmr1*-KO L5 pyramidal neurons transfected with either the β4 subunit shRNA (β4shRNA) or the scramble shRNA (*SI Appendix*, Fig. S4). These findings indicate that altered synaptic integration in the basal dendrites in *Fmr1*-KO L5 pyramidal neurons arises from an increased activity of the regulatory β4 subunit. This increase can be explained by the lack of FMRP-mediated β4 sequestering in *Fmr1*-KO mice (30) leading to an elevated binding of the β4 subunit to BK channels impacting the integration of incoming synaptic inputs in the basal dendrites L5 pyramidal neurons.

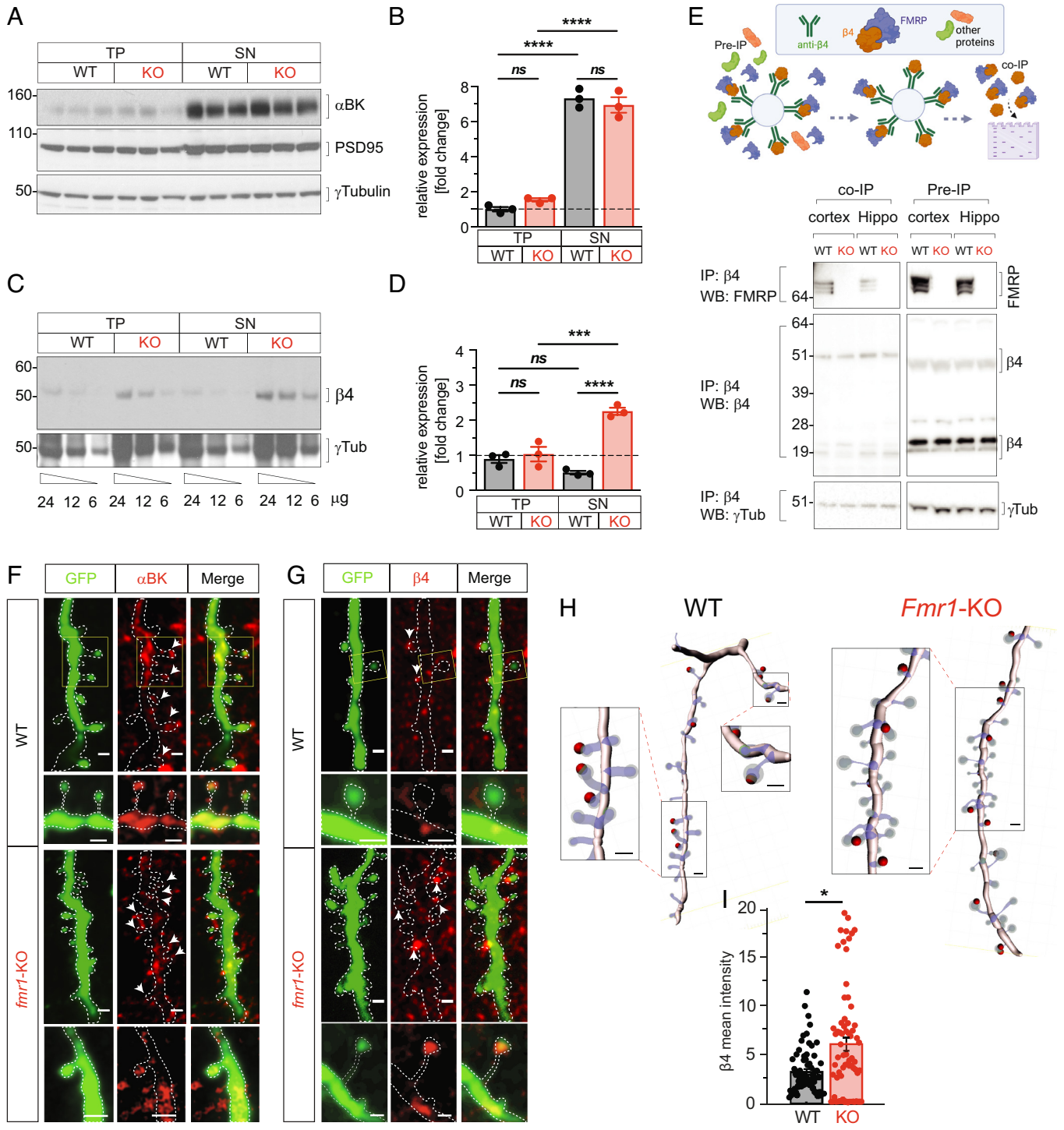

Fig. 2. Expression of αBK and β4 subunits in synapses of *Fmr1*-KO mice. (*A* and *B*) Mouse visual cortex TP and Synaptoneurosome (SN) fractions were analyzed by western blot with specific monoclonal antibodies and normalized by the expression of γ-tubulin. (*A*) Expression of αBK (20 µg/line). Synaptic enrichment in the SN fraction was confirmed by the expression of the postsynaptic density (PSD) marker PSD95. (*B*) αBK expression normalized by γ-tubulin and by the expression in WT/TP (n = 3, $P < 0.0001$, ANOVA). (*C*) Expression of β4. A mix of three samples for each condition was loaded at decreasing concentrations (24, 12, 6 µg/line). (*D*) β4 expression normalized by γ-tubulin and by the expression in WT/TP (n = 3, $P < 0.05$, $P < 0.0001$, ANOVA). (*E*) Representation of the experimental workflow (see *Methods*) and blots corresponding to co-IP of FMRP, immunoprecipitation (IP) of β4 and the loading control γ-tubulin (200 µg/sample input protein). Left side of the bottom panel, co-IP Western blot performed using anti-β4 antibody to precipitate and detect a protein complex containing FMRP bound to β4 subunit in the visual cortex and hippocampus of *Fmr1*-KO and control mice P25±1 (n = 3, pooled samples). Right side (pre-IP) shows the composition of the original sample (16 µg/line). (*F–I*) Expression of channel subunits in excitatory synapses was studied in P26±1 *Fmr1*-KO and control transgenic mice expressing GFP in L5 pyramidal neuron (green) by immunofluorescent detection of αBK (*F*) and β4 subunits (red) (*G*) Dendritic spine channel expression is shown in one <1-µm confocal optical slice. Arrow heads indicate spines with detectable expression of the BK subunit. *Insets* (yellow boxes) and additional examples at higher magnification are shown below each group with clear αBK or β4 subunit spine localization. (Scale bar, 1 µm.) (*H*) Examples of dendrite 3D reconstructions from the same neurons shown in *G*), above threshold β4 subunit immunoreactivity and signal overlapping with the spine head are shown as red dots. (*I*) Mean intensity of the β4 subunit signal in each spine head was compared between *Fmr1*-KO and control mice. (*Fmr1*-KO, n = 206 spines, WT, n = 143 spines, $P < 0.05$, Mann–Whitney test).

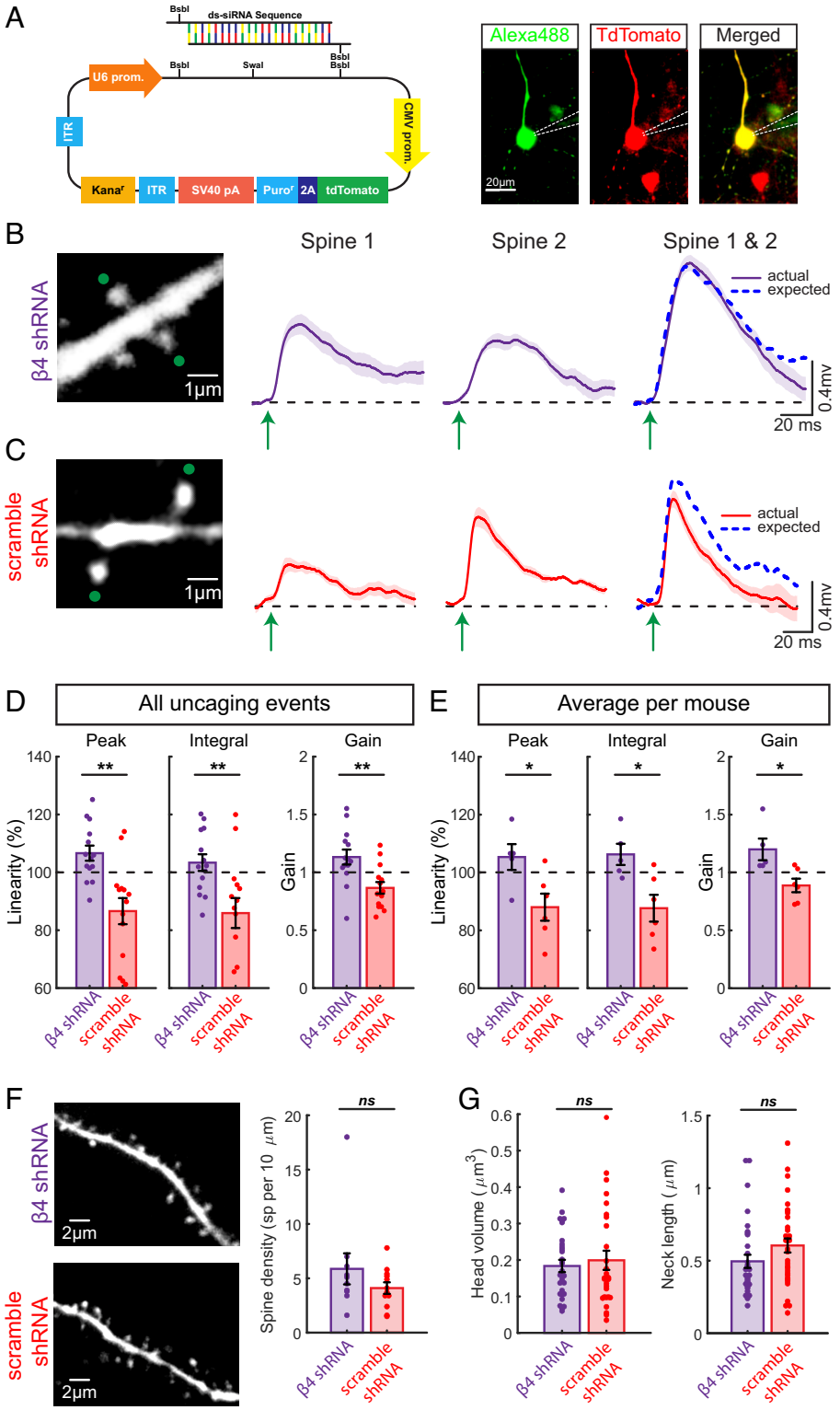

Fig. 3. Knock-down of β4 subunit of BK channels rescues sublinearity of synaptic inputs in the basal dendrites of *Fmr1*-KO L5 pyramidal neurons. (*A*) Schematic of the shRNA vector used to knockdown β4. (*B* and *C*) shRNA knock-down of the β4 subunit of BK channels rescues the sublinearity in the basal dendrites of *Fmr1*-KO L5 pyramidal neurons (*B*) while injection of scrambled shRNA has no effect (*C*). (*D*) Observed responses were not significantly different in amplitude, integral, and gain than that expected based on the sum of individual responses in *Fmr1*-KO mice injected with the β4shRNA, while those injected with a scrambled version, the responses summate sublinearly. (*E*) As in D, but values were averaged per mouse. (*F* and *G*) Spine density (*F*) and spine morphology (*G*) are not significantly different in *Fmr1*-KO L5 pyramidal neurons injected with shRNA targeted to the β4 subunit of BK channels versus nonspecific scrambled shRNA in L5 of the visual cortex.

Biophysical Simulations of Synaptic Integration in Basal Dendrites of *Fmr1*-KO and WT L5 Pyramidal Neurons: Increased Number of Synaptically Activated BK Channels upon β4 Subunit Binding in *Fmr1*-KO Mice. To corroborate our experimental observations indicating the interaction of the β4 subunit with BK channels in spines impacts the integration of subthreshold excitatory inputs

in the basal dendrites of L5 pyramidal neurons, and gain detailed information on the mechanistic underpinnings of this process, we turned to multicompartmental simulations in the NEURON environment (47). Briefly, a morphologically realistic L5 pyramidal neuron was built (adapted from refs. 31 and 48) where two spines were simulated with neck lengths of 1 μm and head volumes of 0.18 μm^3, which matched the morphology of spines probed in our 2P experiments (Fig. 4 *A* and *B*). The dendritic spines were connected to a randomly selected basal dendrite located 170 μm away from the soma of the modeled L5 pyramidal neuron. α-amino-3-hydr oxy-5-methyl-4-isoxazolepropionic acid (AMPA)-receptors(R), N-methyl-D-aspartate (NMDA)-receptors(R), voltage-gated calcium channels, sodium channels, and BK channels were placed in the plasma membrane of each spine head compartment (see *Methods*; Fig. 4 *A* and *B*). In one set of simulations, a WT L5 pyramidal neuron was modeled by incorporating the activation/deactivation parameters and kinetics of the α-subunit of BK channels, while in another group a *Fmr1*-KO L5 pyramidal neuron was modeled by using those obtained when the β4 subunit is bound to the α-subunit of BK channels (49). We then simulated our 2P experiments by modeling synaptic inputs onto two individual spines separately and then together (Fig. 4 *A* and *B*, *Right*). The simulations show that synaptic integration occurs linearly in the simulated WT neuron, when α-subunit of BK channels in spines are modeled (Fig. 4*A*), while inputs integrate sublinearly in the simulated *Fmr1*-KO neuron when the β4 subunit are incorporated in spines (Fig. 4*B*), emulating our experimental observations. We quantified these results by calculating linearity indices, using either the peak or integral of the EPSP as well as a gain measure (Fig. 4*C*). To understand the mechanistic underpinnings underlying the sublinear integration in *Fmr1*-KO L5 pyramidal neurons, we analyzed the number of open BK channels per spine when one versus two spines were activated in

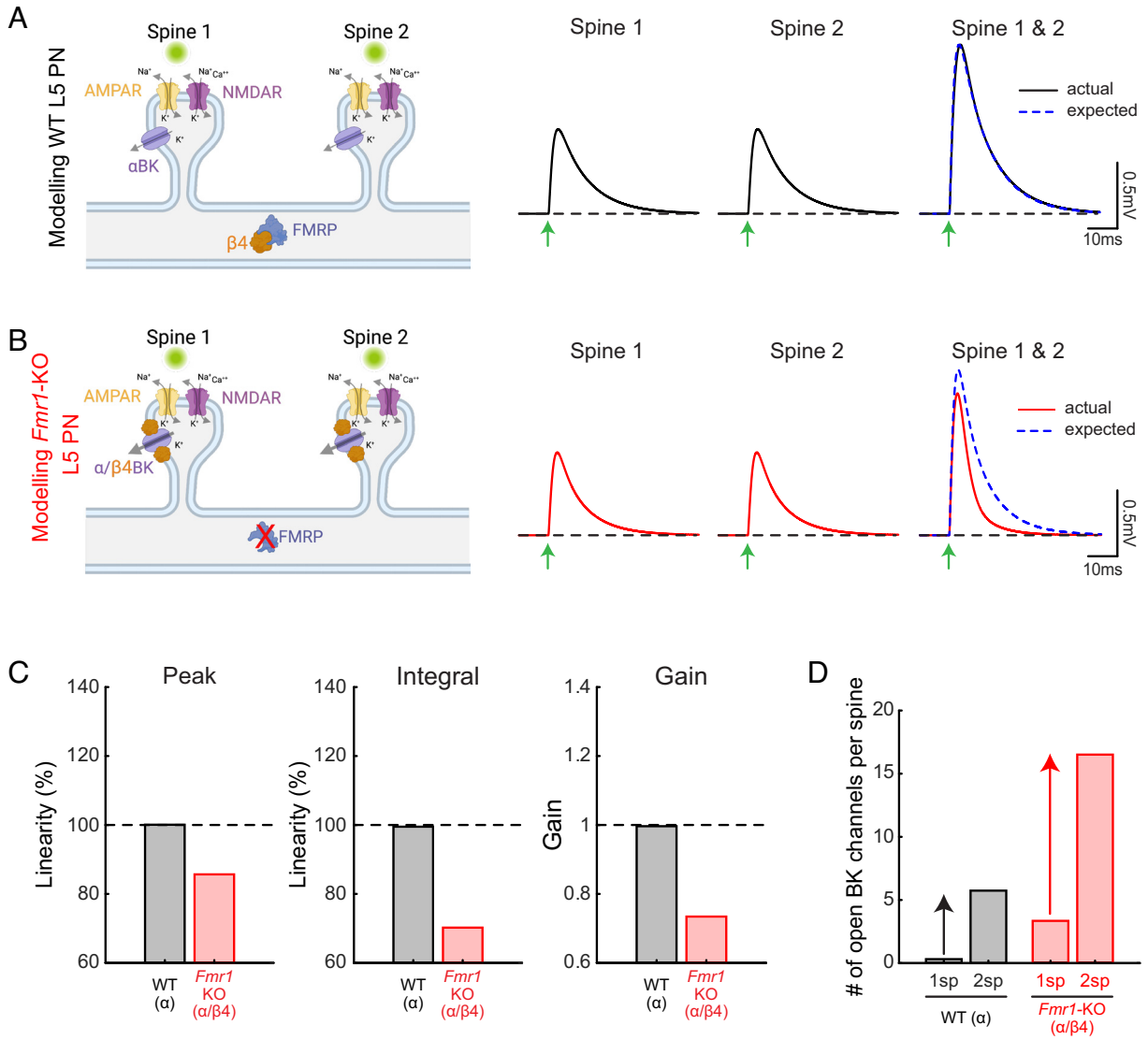

Fig. 4. Biophysical modeling shows the effect of the BK channel β4 subunit on synaptic integration in dendritic spines. (*A* and *B*) *Left* panels: Schematic of the model used to assess synaptic integration in the basal dendrites of a WT L5 pyramidal neuron (*A*) expressing FMRP, which sequesters the β4 subunit so only the α subunit is present in the spine and a *Fmr1*-KO L5 pyramidal neuron (*B*), which does not express FMRP so the β4 subunit is free to bind the BK channel. *Right* panels: Spines were first activated individually (Spine 1 or Spine 2) and then together (Spine 1 & Spine 2), and the EPSP generated at the soma was recorded. Blue dashed traces correspond to the linear sum of individual events of each spine. In the WT neuron, the actual and expected EPSP responses match (compare black and dashed blue traces), whereas in the KO neuron, the actual EPSP response is much less than expected (compare dashed red and blue traces). (*C*) Observed response has smaller amplitude, integral, and gain than the expected based on the sum of individual responses in *Fmr1*-KO neuron, while in WT mice, the responses summate linearly. (*D*) Number of BK channels open during activation of 1 spine or 2 spines in the modeled WT and *Fmr1*-KO L5 pyramidal neuron.

WT versus *Fmr1*-KO L5 pyramidal neurons. Our simulations show that more BK channels are open when two spines are activated, but in the presence of the β4 subunit there is a significantly larger boost in the number of open BK channels per spine (Fig. 4*D*), leading to the sublinear integration of subthreshold excitatory inputs in the basal dendrites—mimicking our experimental results found in *Fmr1*-KO L5 pyramidal neurons (Fig. 1*A*).

Discussion

Previous work suggested that FXS and ASD are characterized by a hyperexcitable neocortex (13–17), thought to be the main contributor to hypersensitivity of sensory stimuli observed in autistic individuals (reviewed in ref. 19). Our experimental findings presented here challenge this generalized view that there is a global hypersensitivity in the neocortex associated with FXS, as they show that the integration of subthreshold excitatory inputs onto the basal dendrites, the main recipients of sensory inputs, of L5 pyramidal neurons in *Fmr1*-KO mouse is sublinear (i.e., combined response smaller than arithmetic sum of individual events). We further studied the mechanism for this sublinear integration. BK channels and their β4 subunit are localized to basal dendritic spines of WT and *Fmr1*-KO L5 pyramidal neurons (Fig. 2) (31) and FMRP (absent in *Fmr1*-KO mice) binds the β4 subunit in the neocortex of WT mice (Fig. 2*E*) thus preventing it from binding to BK channels and altering their activation/deactivation parameters and kinetics (32, 33). We thus investigated how BK channels and their β4 regulatory subunit affect synaptic integration in *Fmr1*-KO L5 pyramidal neurons. We found that a knockdown of the β4 regulatory subunit in *Fmr1*-KO L5 pyramidal neurons rescued linearity from the sublinear integration previously observed in their basal dendrites. Finally, our numerical simulations corroborate these findings, as they show that the linear integration of excitatory synaptic inputs occurs only when the kinetics of the α-subunit of BK channels are modeled, while when the β4 subunit is incorporated the number of open BK channels per spine is boosted, leading to an enhanced repolarization when two spines are activated and sublinear integration of subthreshold excitatory inputs.

To make predictions about the future, the brain has to associate feedforward sensory with feedback predictive information (20–22). Hypersensitivity to sensory stimuli is described as one of the classical symptoms experienced by individuals with FXS and other forms of ASD (reviewed in ref. 19). One might think that being hypersensitive to certain stimuli makes you better able to detect it and perform certain behavioral tasks more aptly, which does not actually seem to consistently be the case for autistic individuals or mouse models of ASD. For example, children with ASD exhibit increased detection thresholds during tactile stimulation (50). While it has been shown that *Fmr1*-KO mice exhibit an enhanced acoustic startle response at low sound intensities; they actually show a decreased response to high-intensity sounds (51, 52). *Fmr1*-KO mice also showed impaired learning in a visual discrimination task and took longer to reach expert-level performance comparable to WT animals (53). Moreover, this study did not find a significant increase in either spontaneous or visually evoked activity in Layer 2/3 pyramidal neurons of *Fmr1*-KO mice. Thus, the results of these behavioral studies are in agreement with those we report here, in that they cannot consistently be explained by hyperexcitability of the cortex to sensory stimuli. Our data show that near simultaneous activation of two spines in the basal dendrites generates a subthreshold depolarization that summates sublinearly in *Fmr1*-KO mice, whereas, in their WT counterparts, this integration occurs in a linear fashion (Fig. 1 and see also ref. 28). The apical dendrites of L5 pyramidal neurons receive contextual information from other brain areas, and exhibit a greater density of hyperpolarization-activated cyclic nucleotide-gated (HCN) channels (54), in contrast to BK channels, which are homogenously distributed across the dendritic tree of L5 pyramidal neurons. The apical dendrites of *Fmr1*-KO pyramidal neurons are hyperexcitable due to an increased impedance caused by the reduction of HCN channels in apical dendrites, resulting in an enhanced temporal summation of excitatory input (13). Thus, taken together, the hypersensitivity characterized in FXS is not simply due to an upweighting of sensory inputs at the level of L5 pyramidal neurons, but instead by a hyposensitivity of sensory inputs and a hypersensitivity of predictive inputs. Specifically, the overrepresentation of predictive inputs onto the apical dendrites of L5 pyramidal neurons, coinciding with a down-representation of sensory inputs at the level of the basal dendrites of cortical pyramidal neurons, may be at the core of the behavioral phenotypes associated with FXS. These changes would likely have significant effects on the input/output properties of L5 pyramidal neurons, and thus in the ability of the cortex to decipher sensory signals in order to make predictions about the future. Moreover, the results from the present study highlight the need to study, in FXS and other forms of ASD, cortical feedforward and feedback pathways independently, their associations, and how they ultimately affect cortical pyramidal neuron's output to shape behavioral learning.

The relevance for the subthreshold activation of clustered spines, synaptic microclusters (38) (~2 to 5 spines), in L5 pyramidal neuron dendrites for representing multiple independent tasks and stabilizing learning has been observed by recent computational studies (55, 56), and is supported by anatomical (57–61) and functional (31, 61–63) observations. Hence, the sublinear integration in spine microclusters would likely affect the threshold for the induction of synaptic plasticity, sensory task representations in basal dendrites, and ultimately learning in *Fmr1*-KO mice.

Although the present study focused on L5 pyramidal neurons in *Fmr1*-KO mice, there have been many studies on how FXS and ASD in general alters the activity of cortical interneurons. Cortical pyramidal neuron activity is modulated by inhibitory interneurons, which control the firing of their postsynaptic target neurons to maintain network activity within a certain range and prevent epileptic episodes (64). Many mouse models of ASD exhibit altered interneuron function and development (65). Specifically, compared with WT animals, *Fmr1*-KO mice displayed delayed learning of a visual discrimination task, and reduced activity of parvalbumin (PV) interneurons in the visual cortex. Restoring PV cell activity accelerated the learning in *Fmr1*-KO mice (53). Moreover, the somatosensory cortex of *Fmr1*-KO mice has a significant reduction in the density of PV neurons (66). Thus, it is likely that the stereotypical behavior observed in FXS is caused by complex alterations in cortical circuits, where both the computations performed by L5 pyramidal neurons integrating feedforward sensory and feedback predictive inputs in addition to their modulation by inhibitory interneurons are impaired (67).

Studies investigating how the BK channel β4 subunit impacts the activity of hippocampal and neocortical pyramidal neurons have shown that FMRP interacts with the β4 subunit [in the hippocampus (30) and in the cortex (Fig. 2*E*)] and that the lack of FMRP leads to excessive broadening of pyramidal neuron action potentials, and consequently their inter-spike-interval during repetitive activity (30). Thus, FMRP can regulate neural firing patterns through a BK channel-mediated mechanism by the interaction of FMRP and the BK channel β4 subunits (30). The effect of the β4 subunit on BK channels is complex as it decreases the

probability of BK channels opening at low intracellular calcium concentrations but promotes channel opening at high intracellular calcium concentrations while also slowing down activation and deactivation kinetics (32, 33). Thus, how the β4 subunit will affect BK channel opening depends on intracellular calcium levels. In the present study, we focused on how the BK channel β4 subunit influences the integration of subthreshold inputs onto spines (i.e., uEPSPs). Our results showing that knockdown of the β4 subunit of BK channels rescues synaptic integration are in agreement with the activation voltage range of BK channels at intracellular calcium levels reached in the spine upon synaptic activation [$V_{1/2}$ of ~−50 mV versus ~−20 mV, for β4-bound BK channels versus unbound, respectively, for intracellular calcium concentration of ~20 μM (49)] and the dendritic spine depolarization generated by activating clustered spine pairs (Fig. 4*D*). How the behavior of these rescued *Fmr1*-KO mice is affected is a future direction of research. Taken together, our results along with previous studies show that in *Fmr1*-KO pyramidal neurons, the β4-bound BK channels causes 1) subthreshold inputs to be integrated sublinearly in the basal dendrites due to a greater repolarization when two spines are activated and 2) alterations in the timing of action potentials and information transmission compared with WT mice (30). Both of these defects can severely influence how sensory information is transmitted to downstream neurons from L5 pyramidal neurons.

This is a demonstration of hyposensitivity of sensory inputs at the level of L5 pyramidal neurons in a mouse model of ASD. Specifically, these results reveal a hyposensitivity of basal integration of sensory inputs in *Fmr1*-KO L5 pyramidal neurons through a mechanism dependent on the interaction between BK channels and β4 subunit. This work adds to our understanding of FXS by demonstrating that it is not solely characterized by a global sensory hypersensitivity at the cellular level and provides instead a more complex picture where the differential integration of feedforward and feedback inputs in L5 pyramidal neurons could be at the core of the cellular basis of FXS.

Materials and Methods

Animals. C57B/6 (WT, RRID:IMSR_JAX:000664) and *Fmr1*-KO (B6.129P2-*Fmr1*^{tm1Cgr}/J, RRID:IMSR_JAX:003025) and *Fmr1*-KO;thy1GFPM (*Fmr1*-KO backcrossed to Tg(Thy1-EGFP)MJrs/J, RRID:IMSR_JAX:007788) mice were used in this study and housed on a 12-h light/dark cycle with ambient temperature 20 to 24 °C and 40 to 70% humidity. Since FXS is more prevalent in males than females, only male mice were used in this study.

Brain Slice Preparation and Electrophysiology. Mice (P14-37), anesthetized with isoflurane, were decapitated, and their brains dissected and placed in cold (4 °C) carbogenated sucrose cutting solution containing (in mM) 27 $NaHCO_3$, 1.5 NaH_2PO_4, 222 sucrose, 2.6 KCl, 1 $CaCl_2$, and 3 $MgSO_4$. Coronal brain slices (300-μm-thick) of the visual cortex were prepared using a Vibratome (VT1000 S, Leica) and slices were incubated for 30 min at 32 °C in Artificial cerebrospinal fluid(ACSF) (in mM: 126 NaCl, 26 $NaHCO_3$, 10 dextrose, 1.15 NaH_2PO_4, 3 KCl, 2 $CaCl_2$, 2 $MgSO_4$) and then at room temperature until ready for use. MultiClamp 700 B amplifiers (Molecular Devices) were used for electrophysiological recordings of L5 pyramidal neurons with a patch electrode (4 to 7 MΩ) filled with internal solution containing (in mM): 0.1 Alexa-568, 130 Potassium D-Gluconic Acid (Potassium Gluconate), 2 $MgCl_2$, 5 KCl, 10 HEPES, 2 MgATP, 0.3 NaGTP, pH 7.4, and 0.4% Biocytin. DIC optics were used to clearly visualize and patch the soma of L5 pyramidal neurons.

Two-Photon Imaging and Two-Photon Uncaging of Glutamate. Two-photon imaging was performed using a custom-built two-photon laser scanning microscope (37, 38), consisting of 1) a Prairie scan head (Bruker) mounted on an Olympus BX51WI microscope with a ×60, 0.9 NA water-immersion objective; 2) a tunable Ti-Sapphire laser (Chameleon Ultra-II, Coherent, >3 W, 140-fs pulses, 80 MHz repetition rate), 3) two photomultiplier tubes (PMTs) for fluorescence detection. Fluorescence images were detected with Prairie View 5.4 software (Bruker).

Fifteen minutes following break-in, two-photon scanning images of basal dendrites were obtained with 720 nm at low-power (<5 mW on sample) excitation light and collected with a PMT. Two-photon uncaging of MNI-caged L-glutamate (2.5 mM; Tocris) was performed using a 4-ms pulse at 720 nm and ~30 mW on sample (28) with the uncaging spot ~0.3 μm away from the upper edge of the selected spine head. The uEPSPs were recorded with the patch pipette at the soma of L5 pyramidal neurons. To assess the integration of individual synaptic inputs onto the basal dendrites of L5 pyramidal neurons, two-photon uncaging of MNI-glutamate was used. Uncaging was performed first at two neighboring spines separately and then together (interstimulus interval of <0.1 ms) with a 2-s delay in between each uncaging event. This sequence was repeated 10 times. Recordings were obtained using a MultiClamp 700B amplifier (Axon Instruments) interfaced to a dedicated computer by a BNC-2090A data acquisition board (National Instruments). The electrophysiological signals were acquired at 10 kHz using the *PackIO* open-source software package (https://github.com/apacker83/PackIO).

Electrophysiology and Imaging Data Analysis. Offline data analysis was performed with the MATLAB (Mathworks) EphysViewer package (https://github.com/apacker83/EphysViewer) and custom written algorithms. We first quantified our results by calculating linearity indices, using either the peak or integral of the uEPSP, as described in the following equations:

$$Linearity_{peak} = \frac{max(uEPSP_{sp1\&sp2})}{max\left(uEPSP_{sp1} + uEPSP_{sp2}\right)} \quad [1]$$

and

$$Linearity_{integral} = \frac{\int uEPSP_{sp1\&sp2}}{\int uEPSP_{sp1} + uEPSP_{sp2}}, \quad [2]$$

where $uEPSP_{sp1}$, $uEPSP_{sp2}$, and $uEPSP_{sp1\&sp2}$ are the time varying uEPSP responses when we applied 2P uncaging of glutamate at spine 1, spine 2, and then together near-simultaneously, respectively.

Linear optimization techniques were also used to quantify the linearity of synaptic inputs for WT and *Fmr1*-KO mice. Specifically, the uEPSP response to near-simultaneous uncaging of neighboring spines was modeled using the following equation:

$$uEPSP_{sp1\&sp2}(t) = gain \times \left(uEPSP_{sp1}(t) + uEPSP_{sp2}(t)\right), \quad [3]$$

where $uEPSP_{sp1}(t)$, $uEPSP_{sp2}(t)$, and $uEPSP_{sp1\&sp2}(t)$ are the time varying uEPSP responses when we applied 2P uncaging of glutamate at spine 1, spine 2, and then together near-simultaneously, respectively and *gain* is a measure of how close the expected (based on the arithmetic sum) and actual responses to uncaging spine 1 and spine 2 are to each other–a measure of linearity of the time-varying uEPSP responses. When only older animals (range P22-37) are considered, we obtain the same statistical results for linearity indices and gain measure of WT versus *Fmr1*-KO L5 pyramidal neurons (peak linearity: 101.7 ± 2.22 versus 91.4 ± 1.67%, $P = 0.0004$; integral linearity: 103.8 ± 2.77 versus 90.9 ± 2.37%, $P = 0.0005$; gain linearity: 1.04 ± 0.03 versus 0.88 ± 0.02, $P = 0.0002$, Mann–Whitney test).

Analysis of the spine morphology was performed in the open source image processing package Fiji (NIH). Specifically, the spine neck was measured as the proximal edge of the spine head to the edge of the dendrite. In cases where the spine topology could not be precisely determined, the spine neck length was estimated as the shortest orthogonal distance between the base of the spine head and the edge of the dendrite. When the spine neck could not be measured, a minimum value of 0.2 μm was used. For the spine head size, the longest and corresponding orthogonal diameter was measured. These measures were computed from a Gaussian curve fit to the fluorescent profile of these axes, generated from a z-stack over the entire spine heads (Δz = 0.4 μm). The corresponding spine head volume (V, in μm^3) was estimated using the following formula:

$$V = \frac{4}{3}\pi\left(\frac{d_{long} + d_{orth}}{2}\right)^3, \quad [4]$$

where d_{long} and d_{orth} are the FWHM of the spine head along the longest and corresponding orthogonal dimension, respectively. The FWHM was calculated using the SD (σ) of the Gaussian curve fit to the fluorescent profile of the spine heads (FWHM = 2.335 σ).

Synaptoneurosome (SN) Preparation. An adaptation of a previously described method was used (68, 69) as follows: P14 mouse visual cortex was dissected, flash frozen, and stored at −80 °C. Individual samples (approx. 1 mg) were homogenized in 700 μL SN lysis buffer (10 mM Hepes, pH 7.4, containing proteinase inhibitor) using a 2-mL Kimble–Chase tissue grinder (Thermo Fisher K885300-0002) and applying six loose pestle and 12 tight pestle strokes. A 150 μL aliquot of this TP fraction was boiled in 10% sodium dodecyl sulfate (SDS) for 10 min and stored. The remaining fraction was centrifuged at 2,000×g for 2 min at 4 °C to remove cellular and nuclear debris. The supernatant was loaded into a 1-mL syringe and filtered through three layers of a prewetted 100-μm pore nylon filter (Millipore NY1H04700). The filtrate was directly loaded into 5-μm-pore centrifugal filters (Ultrafree-CL, Millipore UFC40SV25) and centrifuged at 5,000×g for 15 min in a fixed angle rotor at 4 °C. The supernatant was carefully removed, and the loose pellet resuspended in boiling SN buffer (containing 2% SDS), boiled for 10 min and stored at −80 °C (SN protein fraction). Protein concentration was determined with the Bicinchoninic acid(BCA) protein assay kit (Thermo Fisher 23227) using a bovine serum albumin (BSA) standard curve.

Co-IP. Proteins were prepared adapting a previously described method (70). The flash frozen visual cortex and hippocampus from P25±1 *Fmr1*-KO and control mice were homogenized over ice using a 2-mL glass/glass tissue homogenizer (Kontes, Fisher K885300-0002) in 400 μL ice-cold lysis buffer containing 20 mM Tris (pH 7.4), 200 mM NaCl, 1% NP-40, and proteinase inhibitors. Proteins were then extracted by incubating the homogenate on ice with occasional agitation for 30 min and then centrifugating at 15,000 g for 20 min. The pellet was resuspended in 200 μL lysis buffer, and the extraction step repeated. Both supernatants were pooled, and protein concentration was determined using the BCA method (Pierce 23227). Dynabeads protein G were used as suggested by the manufacturer (Thermo Fisher 10007D): For each sample 50 μL magnetic beads were cross-linked to 5 μg anti-β4 antibody (Antibodies Inc 75-086) with 230 μL 5 mM BS^3 (Thermo Fisher A39266). Samples were incubated with the prepared beads for 16h at 4 °C. The supernatant containing the unbound proteins (post-IP) was stored and the beads washed. Finally, the bound protein (IP) was recovered in 10 μL elution buffer (50 mM Glycine pH 2.8) and used directly for Western blot with the addition of desaturating loading buffer.

Western Blot. An adaptation of a previously described method was used (71) as follows: protein samples were separated in NuPAGE™ 3 to 8% Tris-Acetate Protein Gels (Thermo Fisher EA03755) in Tris-Acetate-EDTA running buffer (Thermo Fisher BP13354) at 200V for 1 h for αBK and Bis-Tris 4 to 12% polyacrylamide gradient gels (Thermo Fisher NP0323, NW0412B) in MES–SDS running buffer (Thermo Fisher B0002) at 200 V for 30 min for β4 subunit. Separated proteins were transferred into a PVDV membrane using a mini trans-blot cell (BioRad 170-3930) at 200V for 1 h for αBK and at 150 V for 50 min for the β4 subunit. Ponceau red staining was performed after transfer and recorded. Membranes were blocked in 0.1% Tween20 in phosphate–buffered saline (PBS) starting block (Thermo Fisher 37538) and incubated with primary antibodies diluted in the same buffer: anti-BK channel 1:500 (Antibodies Inc 75-022) or 1:100 anti-BKbeta4 potassium channel (Antibodies Inc 75-086) and after striping a mix of anti-γ-tubulin 1:10,000 (Sigma-Aldrich,T5326,) and anti-PSD95 1:5,000 (Antibodies Inc 75-028), in addition, for the Co-IP: 1:1,000 anti-FMRP (Clone 2F5, a gift from the Darnell lab) and 1:500 anti-β4 (KCNMB4) (Alomone APC-061). Signal was developed using ECL substrate (BioRad 170-5060) and recorded on film or using a bio imager. Densitometric analysis was performed with the open-source program FIJI (72), and data were plotted using Prism9 (GraphPad).

Immunofluorescence. Anesthetized P25-27 *Fmr1*-KO;thy1GFPM mice were intracardially perfused with 4% PFA in PBS. Postfixing of the brain was done in 4% PFA for 2 h at 4 °C followed by washes in PBS and dehydrated in 30% sucrose at 4 °C and then mounted in OCT by freezing in a bath of 2-methylbutane at −50 °C. The 40-μm cryosections were cut at −18 °C and placed over glass slides treated with tissue capture pen (Electron Microscopy Sciences 71314) and stored at −80 °C. Cryosections were permeabilized and blocked in TSA blocking reagent (Perkin Elmer FP1020). Primary antibodies used were anti-BK 1:100 (Antibodies Inc AB_224953), 1:300-1:100 anti-BKbeta4 potassium channel (Antibodies Inc 75-086) and anti-GFP 1:500 (Rockland 600-101-215). Incubations were performed for 16 h at 4 °C followed by incubation with secondary antibodies: Alexa 568 anti-mouse 1:200 (Thermo Fisher A10037), and Alexa 488 anti-goat 1:200 (Thermo Fisher A11055) for 2 h at room temperature (RT) in TSA blocking reagent. Washes were done in PBS. The samples were mounted in ProLong Diamond Antifade Mountant with DAPI (Thermo Fisher P36971) or Vectashield (Vector Labs H-1200), and the basal dendrites from L5 pyramidal neurons were imaged using a Zeiss LSM700 confocal microscope (IRIC bio-imaging core). Each optical slice was 0.7 to 1.0-μm thick.

Image Processing for Immunofluorescence Experiments. The Laser Scanning Microscopy (LSM) toolbox Fiji (72) plugin was used to process the confocal images as follows: Raw images saved in LSM format were opened and optical slices of the z stack with good dendritic morphology observed in the green (GFP) channel were duplicated (to extract one slice), rotated, and cropped. Red (αBK or β4 subunit) and green channels were separated with the color split function and contrast and brightness were manually adjusted to achieve clear images of similar intensity in both channels. Gaussian blur set at 1 to 2 (the same for both channels) was then applied to smooth the pixels. Both channels were stacked using the color merge channel function, which generates a yellow color (merge) in overlapping areas of similar intensity. Scale bars were automatically drawn using the LSM bar tool function.

For quantitative analysis of β4 subunit expression in spine heads, Imaris software (Oxford Instruments version 9.8) was used for semi-automatic dendrite and spine reconstruction of the GFP signal, followed by spine head object generation with a MATLAB tracking plugin (total spine heads). Dots generated from the β4 channel signal overlapping with spine heads were selected, and their mean intensity determined. In addition, the data were used to calculate the percentage of spines with detectable signal. We discarded the signal in the spine neck because the confocal images of transgenic GFP did not allow for a good estimation of the real shape and volume.

Virus Injection. To perform the knockdown of the β4 subunit of BK channels, a mix of two different AAV1 were used, each containing a different shRNA based on kcnmb4 the mouse sequence (NM_021452): shkcnb4-NM_021452.126s1c1: 5′-CCGGCCCGCCUUGCAGGAUCUGCAACUCGAGUUGCAGAUCCUGCAAGGCGGGUUUUUG-3′ (binding nucleotides 126 to 146) and shkcnb4_NM_021452.1-266s1c: 5′-CCGGCGUGAACAACUCCGAGUCCAACUCGAGUUGGACUCGGAGUUGUUCACGUUUUUG-3′ (binding nucleotides 266-189) or a control custom scramble shRNA: 5′-CCGGACCACCGTCGAATCGTGACAACTCGAGTTGTCACGATTCGACGGTGGTTTTTTG-3′ cloned downstream of the U6 promoter in a pAAV-shRNA-tdTomato vector and prepared at a concentration of 10×10^{13} GC/mL (abm, Canada). The morning of the surgery, *Fmr1*-KO mice (P18) were given sustained-release buprenorphine (1 mg/kg). Mice were then deeply anesthetized with 3% isoflurane, confirmed by the absence of a toe pinch response and placed into a stereotaxic frame (Kopf Instruments). An incision was made into the disinfected bare skin to expose lambda and bregma landmarks. A small hole was drilled into each side of the skull at 3 mm posterior and 2 mm lateral to the bregma. The virus was loaded into a Hamilton syringe and injected 0.5 mm below the pial surface. The virus (450 μL) was injected bilaterally, over the course of 20 min followed by a 5-min wait period before the syringe was slowly and carefully removed. The incision was sutured and mice were returned to their home cage and given 2 wk to recover and obtain a good virus expression. 2P uncaging experiments, as described above, were performed on L5 pyramidal neurons expressing the reporter gene tdTomato.

Modeling. We used a morphologically realistic L5 pyramidal neuron NEURON model (31, 48) to study the effects of the β4 subunit on synaptic integration. Two spines, with neck lengths of 1 μm and spine head volumes of 0.18 μm^3, were inserted 170 μm from the soma on a randomly selected basal dendrite. The neck width was estimated based on the head volume using previously reported linear relationships that found a positive correlation between head size and neck width in distal dendrites (7), also been observed in-vivo using Stimulated emission depletion (STED) nanoscopy (73) and other cortical

pyramidal neurons (74). Neck and spine head axial resistances were set to 500 and 150 MΩ, respectively, based on published values (75, 76). High voltage-activated (HVA) calcium channels (https://senselab.med.yale.edu/modeldb/ShowModel?model=135787&file=/ShuEtAl20062007/ca.mod#tabs-2), calcium buffering/removal mechanisms [resting concentration of 1nM (77)], Nav1.6 sodium channels [4 S/cm^2 (78)], and BK channels (14 S/cm^2) (31, 49) were inserted in the spine heads. In one set of simulations, we incorporated the activation/deactivation parameters and kinetics of the α-subunit of BK channels, while in another set of simulations we used those obtained when the β4 subunit is bound to BK channels (49). To activate individual synapses, we used an ionotropic glutamate receptor stimulation mechanism (79) such that AMPA-R and NMDA-R conductances (10 nS and 0.086 nS, respectively) were calibrated to obtain physiologically realistic EPSPs at the soma (~0.5 to 0.6 mV).

Ethics. These studies were performed in compliance with experimental protocols (13-185, 15-002, 16-011, 17-012, 18-011, and 19-018) approved by the Comité de déontologie de l'expérimentation sur les animaux of the University of Montreal and protocol 2020-2634 approved by the Comité institutionnel des bonnes pratiques animales en recherche of the Centre de Recherche, CHU Ste-Justine.

Data, Materials, and Software Availability. All study data are included in the article and/or *SI Appendix*.

ACKNOWLEDGMENTS. We thank Hélène Klein for excellent technical assistance and are grateful to all other members of Roberto Araya's laboratory for helpful discussions. We thank E. Cook and G. Di Cristo for insightful comments, critical discussion, and reading of the manuscript. Confocal microscopy experiments were carried out at the IRIC Bio-Imaging Core. This work was funded by the Canadian Institutes of Health Research (CIHR) grants MOP-133711 and MOP-377520 to R.A., a Canada Foundation for Innovation (CFI) equipment grant Fonds des leaders 29970 to R.A., a Natural Sciences and Engineering Research Council of Canada (NSERC) Discovery grant #418113-2012, and a Scottish Rite Charitable Foundation of Canada (SRCFC) research grant to R.A. M.B. was supported by a Herber Jesper postdoctoral fellowship at Université de Montréal. D.E.M. was supported by postdoctoral fellowships from the Fonds de recherche du Québec Santé (FRQS) and the Quebec Autism Research Training (QART) Program.

Author affiliations: [a]Department of Neurosciences, Faculty of Medicine, University of Montreal, Montréal QC H3T 1C5, Canada; and [b]CHU Ste-Justine Research Center, Montréal, QC H3T 1C5, Canada

1. S. Jacquemont, R. J. Hagerman, P. J. Hagerman, M. A. Leehey, Fragile-X syndrome and fragile X-associated tremor/ataxia syndrome: Two faces of FMR1. *Lancet Neurol.* **6**, 45–55 (2007).
2. T. Wang, S. M. Bray, S. T. Warren, New perspectives on the biology of fragile X syndrome. *Curr. Opin. Genet. Dev.* **22**, 256–263 (2012).
3. C. E. Rice, "Encyclopedia of autism spectrum disorders" in *Time Trends in Diagnosis*, F. R. Volkmar, Ed. (Springer, New York, 2013), pp. 3120–3125.
4. J. C. Darnell *et al.*, FMRP stalls ribosomal translocation on mRNAs linked to synaptic function and autism. *Cell* **146**, 247–261 (2011).
5. C. R. Hale *et al.*, FMRP regulates mRNAs encoding distinct functions in the cell body and dendrites of CA1 pyramidal neurons. *Elife* **10**, e71892 (2021).
6. M. Colonnier, Synaptic patterns on different cell types in the different laminae of the cat visual cortex. An electron microscope study. *Brain Res.* **9**, 268–287 (1968).
7. J. I. Arellano, R. Benavides-Piccione, J. Defelipe, R. Yuste, Ultrastructure of dendritic spines: Correlation between synaptic and spine morphologies. *Front Neurosci.* **1**, 131–143 (2007).
8. E. G. Gray, Electron microscopy of synaptic contacts on dendrite spines of the cerebral cortex. *Nature* **183**, 1592–1593 (1959).
9. R. D. Rudelli *et al.*, Adult fragile X syndrome. Clinico-neuropathologic findings. *Acta Neuropathol.* **67**, 289–295 (1985).
10. S. A. Irwin *et al.*, Abnormal dendritic spine characteristics in the temporal and visual cortices of patients with fragile-X syndrome: A quantitative examination. *Am. J. Med. Genet.* **98**, 161–167 (2001).
11. C. Portera-Cailliau, Which comes first in fragile X syndrome, dendritic spine dysgenesis or defects in circuit plasticity? *Neuroscientist* **18**, 28–44 (2012).
12. C. X. He, C. Portera-Cailliau, The trouble with spines in fragile X syndrome: Density, maturity and plasticity. *Neuroscience* **251**, 120–128 (2013).
13. Y. Zhang *et al.*, Dendritic channelopathies contribute to neocortical and sensory hyperexcitability in Fmr1-(/y) mice. *Nat. Neurosci.* **17**, 1701–1709 (2014).
14. S. A. Booker *et al.*, Altered dendritic spine function and integration in a mouse model of fragile X syndrome. *Nat. Commun.* **10**, 4813 (2019).
15. I. Bureau, G. M. Shepherd, K. Svoboda, Circuit and plasticity defects in the developing somatosensory cortex of FMR1 knock-out mice. *J. Neurosci.* **28**, 5178–5188 (2008).
16. J. R. Gibson, A. F. Bartley, S. A. Hays, K. M. Huber, Imbalance of neocortical excitation and inhibition and altered UP states reflect network hyperexcitability in the mouse model of fragile X syndrome. *J. Neurophysiol.* **100**, 2615–2626 (2008).
17. S. Rotschafer, K. Razak, Altered auditory processing in a mouse model of fragile X syndrome. *Brain Res.* **1506**, 12–24 (2013).
18. J. T. Goncalves, J. E. Anstey, P. Golshani, C. Portera-Cailliau, Circuit level defects in the developing neocortex of Fragile X mice. *Nat. Neurosci.* **16**, 903–U166 (2013).
19. X. Liu, V. Kumar, N. P. Tsai, B. D. Auerbach, Hyperexcitability and homeostasis in fragile X syndrome. *Front Mol. Neurosci.* **14**, 805929 (2021).
20. M. Larkum, A cellular mechanism for cortical associations: An organizing principle for the cerebral cortex. *Trends Neurosci.* **36**, 141–151 (2013).
21. D. J. Felleman, D. C. Van Essen, Distributed hierarchical processing in the primate cerebral cortex. *Cereb. Cortex* **1**, 1–47 (1991).
22. S. Shipp, Structure and function of the cerebral cortex. *Curr. Biol.* **17**, R443–R449 (2007).
23. A. Soltani, C. Koch, Visual saliency computations: Mechanisms, constraints, and the effect of feedback. *J. Neurosci.* **30**, 12831–12843 (2010).
24. A. Pascual-Leone, V. Walsh, Fast backprojections from the motion to the primary visual area necessary for visual awareness. *Science* **292**, 510–512 (2001).
25. V. A. Lamme, H. Super, H. Spekreijse, Feedforward, horizontal, and feedback processing in the visual cortex. *Curr. Opin. Neurobiol.* **8**, 529–535 (1998).
26. M. Boly *et al.*, Preserved feedforward but impaired top-down processes in the vegetative state. *Science* **332**, 858–862 (2011).
27. N. Takahashi, T. G. Oertner, P. Hegemann, M. E. Larkum, Active cortical dendrites modulate perception. *Science* **354**, 1587–1590 (2016).
28. R. Araya, K. B. Eisenthal, R. Yuste, Dendritic spines linearize the summation of excitatory potentials. *Proc. Natl. Acad. Sci. U.S.A.* **103**, 18799–18804 (2006).
29. P. Y. Deng, V. A. Klyachko, Channelopathies in fragile X syndrome. *Nat. Rev. Neurosci.* **22**, 275–289 (2021).
30. P. Y. Deng *et al.*, FMRP regulates neurotransmitter release and synaptic information transmission by modulating action potential duration via BK channels (vol. 77, pg 696, 2013). *Neuron* **78**, 205 (2013).
31. S. Tazerart *et al.*, Selective activation of BK channels in small-headed dendritic spines suppresses excitatory postsynaptic potentials. *J. Physiol.* **600**, 2165–2187 (2022).
32. R. Brenner, T. J. Jegla, A. Wickenden, Y. Liu, R. W. Aldrich, Cloning and functional characterization of novel large conductance calcium-activated potassium channel beta subunits, hKCNMB3 and hKCNMB4. *J. Biol. Chem.* **275**, 6453–6461 (2000).
33. Y. P. Torres, F. J. Morera, I. Carvacho, R. Latorre, A marriage of convenience: Beta-subunits and voltage-dependent K+ channels. *J. Biol. Chem.* **282**, 24485–24489 (2007).
34. M. Matsuzaki *et al.*, Dendritic spine geometry is critical for AMPA receptor expression in hippocampal CA1 pyramidal neurons. *Nat. Neurosci.* **4**, 1086–1092 (2001).
35. R. Araya, J. Jiang, K. B. Eisenthal, R. Yuste, The spine neck filters membrane potentials. *Proc. Natl. Acad. Sci. U.S.A.* **103**, 17961–17966 (2006).
36. R. Araya, T. P. Vogels, R. Yuste, Activity-dependent dendritic spine neck changes are correlated with synaptic strength. *Proc. Natl. Acad. Sci. U.S.A.* **111**, E2895–E2904 (2014).
37. D. E. Mitchell, E. Martineau, S. Tazerart, R. Araya, Probing single synapses via the photolytic release of neurotransmitters. *Front Synaptic. Neurosci.* **11**, 19 (2019).
38. S. Tazerart, D. E. Mitchell, S. Miranda-Rottmann, R. Araya, A spike-timing-dependent plasticity rule for dendritic spines. *Nat. Commun.* **11**, 4276 (2020).
39. E. Fino *et al.*, RuBi-glutamate: Two-photon and visible-light photoactivation of neurons and dendritic spines. *Front Neural. Circuits* **3**, 2 (2009).
40. R. Araya, Input transformation by dendritic spines of pyramidal neurons. *Front. Neuroanat.* **8**, 141 (2014).
41. R. Araya, V. Andino-Pavlovsky, R. Yuste, R. Etchenique, Two-photon optical interrogation of individual dendritic spines with caged dopamine. *ACS Chem. Neurosci.* **4**, 1163–1167 (2013).
42. E. A. Nimchinsky, A. M. Oberlander, K. Svoboda, Abnormal development of dendritic spines in FMR1 knock-out mice. *J. Neurosci.* **21**, 5139–5146 (2001).
43. T. Bock, G. J. Stuart, The impact of BK channels on cellular excitability depends on their subcellular location. *Front. Cell Neurosci.* **10**, 206 (2016).
44. R. Latorre *et al.*, Molecular determinants of BK channel functional diversity and functioning. *Physiol. Rev.* **97**, 39–87 (2017).
45. M. Matsuzaki, N. Honkura, G. C. R. Ellis-Davies, H. Kasai, Structural basis of long-term potentiation in single dendritic spines. *Nature* **429**, 761–766 (2004).
46. J. Tonnesen, G. Katona, B. Rozsa, U. V. Nagerl, Spine neck plasticity regulates compartmentalization of synapses. *Nat. Neurosci.* **17**, 678–685 (2014).
47. M. L. Hines, N. T. Carnevale, The NEURON simulation environment. *Neural. Comput.* **9**, 1179–1209 (1997).
48. T. Nevian, M. E. Larkum, A. Polsky, J. Schiller, Properties of basal dendrites of layer 5 pyramidal neurons: A direct patch-clamp recording study. *Nat. Neurosci.* **10**, 206–214 (2007).
49. D. B. Jaffe, B. Wang, R. Brenner, Shaping of action potentials by type I and type II large-conductance Ca(2)+-activated K+ channels. *Neuroscience* **192**, 205–218 (2011).
50. N. A. Puts, E. L. Wodka, M. Tommerdahl, S. H. Mostofsky, R. A. Edden, Impaired tactile processing in children with autism spectrum disorder. *J. Neurophysiol.* **111**, 1803–1811 (2014).
51. D. M. Nielsen, W. J. Derber, D. A. McClellan, L. S. Crnic, Alterations in the auditory startle response in Fmr1 targeted mutant mouse models of fragile X syndrome. *Brain Res.* **927**, 8–17 (2002).
52. L. Chen, M. Toth, Fragile X mice develop sensory hyperreactivity to auditory stimuli. *Neuroscience* **103**, 1043–1050 (2001).
53. A. Goel *et al.*, Impaired perceptual learning in a mouse model of Fragile X syndrome is mediated by parvalbumin neuron dysfunction and is reversible. *Nat. Neurosci.* **21**, 1404–1411 (2018).
54. S. E. Atkinson, S. R. Williams, Postnatal development of dendritic synaptic integration in rat neocortical pyramidal neurons. *J. Neurophysiol.* **102**, 735–751 (2009).
55. T. Limbacher, R. Legenstein, Emergence of stable synaptic clusters on dendrites through synaptic rewiring. *Front. Comput. Neurosci.* **14**, 57 (2020).

56. J. Bono, C. Clopath, Modeling somatic and dendritic spike mediated plasticity at the single neuron and network level. *Nat. Commun.* **8**, 706 (2017).
57. H. Schmidt *et al.*, Axonal synapse sorting in medial entorhinal cortex. *Nature* **549**, 469–475 (2017).
58. N. Kasthuri *et al.*, Saturated reconstruction of a volume of neocortex. *Cell* **162**, 648–661 (2015).
59. E. B. Bloss *et al.*, Single excitatory axons form clustered synapses onto CA1 pyramidal cell dendrites. *Nat. Neurosci.* **21**, 353–363 (2018).
60. K. F. Lee, C. Soares, J. P. Thivierge, J. C. Beique, Correlated synaptic inputs drive dendritic calcium amplification and cooperative plasticity during clustered synapse development. *Neuron* **89**, 784–799 (2016).
61. K. S. Lee, K. Vandemark, D. Mezey, N. Shultz, D. Fitzpatrick, Functional synaptic architecture of callosal inputs in mouse primary visual cortex. *Neuron* **101**, 421–428.e425 (2019).
62. B. Scholl, D. E. Wilson, D. Fitzpatrick, Local order within global disorder: Synaptic architecture of visual space. *Neuron* **96**, 1127–1138 (2017).
63. D. E. Wilson *et al.*, Gabaergic neurons in ferret visual cortex participate in functionally specific networks. *Neuron* **93**, 1058-+ (2017).
64. B. R. Ferguson, W. J. Gao, P. V. Interneurons, Critical regulators of E/I balance for prefrontal cortex-dependent behavior and psychiatric disorders. *Front. Neural. Circuits* **12**, 37 (2018).
65. J. W. Lunden, M. Durens, A. W. Phillips, M. W. Nestor, Cortical interneuron function in autism spectrum condition. *Pediatr. Res.* **85**, 146–154 (2019).
66. L. Selby, C. Zhang, Q. Q. Sun, Major defects in neocortical GABAergic inhibitory circuits in mice lacking the fragile X mental retardation protein. *Neurosci. Lett.* **412**, 227–232 (2007).
67. A. Contractor, I. M. Ethell, C. Portera-Cailliau, Cortical interneurons in autism. *Nat. Neurosci.* **24**, 1648–1659 (2021).
68. L. E. Villasana, E. Klann, M. V. Tejada-Simon, Rapid isolation of synaptoneurosomes and postsynaptic densities from adult mouse hippocampus. *J. Neurosci. Methods* **158**, 30–36 (2006).
69. J. Seibt *et al.*, Protein synthesis during sleep consolidates cortical plasticity in vivo. *Curr. Biol.* **22**, 676–682 (2012).
70. E. K. Wittmack *et al.*, Fibroblast growth factor homologous factor 2B: Association with Nav1.6 and selective colocalization at nodes of Ranvier of dorsal root axons. *J. Neurosci.* **24**, 6765–6775 (2004).
71. S. Miranda-Rottmann, A. S. Kozlov, A. J. Hudspeth, Highly specific alternative splicing of transcripts encoding BK channels in the chicken's cochlea is a minor determinant of the tonotopic gradient. *Mol. Cell Biol.* **30**, 3646–3660 (2010).
72. J. Schindelin *et al.*, Fiji: An open-source platform for biological-image analysis. *Nat. Methods* **9**, 676–682 (2012).
73. H. Steffens *et al.*, Stable but not rigid: Chronic in vivo STED nanoscopy reveals extensive remodeling of spines, indicating multiple drivers of plasticity. *Sci. Adv.* **7** (2021).
74. N. Ofer, D. R. Berger, N. Kasthuri, J. W. Lichtman, R. Yuste, Ultrastructural analysis of dendritic spine necks reveals a continuum of spine morphologies. *Dev. Neurobiol.* **81**, 746–757 (2021).
75. C. O'Donnell, M. F. Nolan, M. C. van Rossum, Dendritic spine dynamics regulate the long-term stability of synaptic plasticity. *J. Neurosci.* **31**, 16142–16156 (2011).
76. M. T. Harnett, J. K. Makara, N. Spruston, W. L. Kath, J. C. Magee, Synaptic amplification by dendritic spines enhances input cooperativity. *Nature* **491**, 599–602 (2012).
77. A. Destexhe, A. Babloyantz, T. J. Sejnowski, Ionic mechanisms for intrinsic slow oscillations in thalamic relay neurons. *Biophys. J.* **65**, 1538–1552 (1993).
78. J. N. Mercer, C. S. Chan, T. Tkatch, J. Held, D. J. Surmeier, Nav1.6 sodium channels are critical to pacemaking and fast spiking in globus pallidus neurons. *J. Neurosci.* **27**, 13552–13566 (2007).
79. A. Polsky, B. Mel, J. Schiller, Encoding and decoding bursts by NMDA spikes in basal dendrites of layer 5 pyramidal neurons. *J. Neurosci.* **29**, 11891–11903 (2009).